OPEN

PRS GLOBAL OPEN

EXPERIMENTAL

Oxidative Stress Alters Angiogenic and Antimicrobial Content of Extracellular Vesicles and Improves Flap Survival

John S. Mayo, MD*
Wendy E. Kurata, MS†
Kelsey M. O'Connor, BS†
Lisa M. Pierce, DSc†

Background: Extracellular vesicles (EVs) secreted from adipose-derived mesenchymal stem cells (ADSCs) (ADSC-EVs) improve flap survival after ischemia–reperfusion injury. Exposure of parent ADSCs to oxidative stress has been shown to enhance this effect, but mechanisms are unclear. We aimed to determine whether angiogenesis-promoting protein and microRNA (miRNA) content is altered in EVs after preconditioning with hydrogen peroxide (H_2O_2 ADSC-EVs) and whether H_2O_2 ADSC-EVs can increase viability of random pattern skin flaps.

Methods: EVs secreted by human ADSCs were isolated after culture in EV-depleted medium ± H_2O_2. Nanoparticle tracking analysis determined size and concentration of purified EVs. Mass spectrometry and small RNA next-generation sequencing were performed to compare proteomic and miRNA profiles. ADSC-EVs, H_2O_2 ADSC-EVs, or vehicle were injected into random pattern skin flaps of BALB/c mice (4–5 mice per group). Viable and necrotic areas were measured on day 7, and tissues underwent histologic analysis.

Results: Angiogenic and antimicrobial protein content of EVs was altered with H_2O_2 preconditioning. Functional enrichment analysis identified constitutive photomorphogenesis 9 signalosome (known to direct vascular endothelial growth factor production) as the major enriched Gene Ontology term unique to H_2O_2 ADSC-EVs. Two miRNAs were increased, and 12 (including 10 antiangiogenic miRNAs) were reduced in H_2O_2 ADSC-EVs. Enhanced viability ($P < 0.05$) of flaps treated with H_2O_2 ADSC-EVs compared with vehicle corresponded to increased capillary density in the H_2O_2 group ($P < 0.001$).

Conclusion: Altered protein and miRNA content in ADSC-EVs after H_2O_2 pretreatment likely contributes to enhanced therapeutic effects on flap survival observed in preclinical models. *(Plast Reconstr Surg Glob Open 2019;7:e2588; doi: 10.1097/GOX.0000000000002588; Published online 19 December 2019.)*

INTRODUCTION

Flap necrosis is a serious complication following reconstructive surgery for soft tissue coverage, with treatment at times requiring a return to the operating room or prolonged wound care.[1] Inadequate neovascularization and insufficient production of pro-angiogenic mediators are likely culprits for the poor healing. Injection of adipose-derived mesenchymal stem cells (ADSCs) into skin flaps has been shown by several investigators to increase flap survival and angiogenesis in various skin flap models.[2–5] Recently, extracellular vesicles (EVs) released from ADSCs as a cell-free alternative were also found to improve flap viability after ischemia–reperfusion injury.[6] Bai et al determined that exposure of parent ADSCs to oxidative stress via a low concentration of hydrogen peroxide (H_2O_2) enhanced the angiogenic effects of the EVs, but the mechanisms by which this occurs remain unclear.[7]

The beneficial effects of mesenchymal stem cell (MSC)-based therapies have been proposed to be mediated predominantly by paracrine activity, to include soluble factors and EVs secreted from MSCs.[8–11] EVs are

*From the *Department of General Surgery, Tripler Army Medical Center, Honolulu, Hawaii; and †Department of Clinical Investigation, Tripler Army Medical Center, Honolulu, Hawaii.*

Received for publication August 29, 2019; accepted October 23, 2019.

Presented at Plastic Surgery the Meeting (ASPS) 2019 in San Diego, CA, September 20–23, 2019.

Supported by internal funds from the Department of Clinical Investigation at Tripler Army Medical Center, Honolulu, Hawaii.

DOI: 10.1097/GOX.0000000000002588

Disclosure: *The views expressed in this article are those of the authors and do not reflect the official policy or position of the Department of the Army, Department of Defense, or the US Government. The authors have no financial interest to declare in relation to the content of this article.*

composed of different types of vesicles including exosomes (40–200 nm), which are of endosomal origin, and microvesicles (150–1,000 nm), which directly bud from the cell membrane.[8–11] Because current isolation methods cannot physically separate exosomes from small microvesicles, the term "EVs" in this manuscript refers to vesicles in the size range of exosomes. MSCs have been shown to release EVs that can selectively package and transfer proteins, nucleic acids including microRNAs (miRNAs), and lipids to injured tissues which are capable of modulating gene expression and the biological activity of recipient cells.[8–11] MiRNAs are an important class of highly conserved, small (~22 nucleotide), nonprotein-coding RNAs that regulate gene expression via degradation or translational repression of their targeted mRNA transcripts.[12] They are significant modulators of numerous fundamental physiological and cellular processes including angiogenesis, and their dysregulation is implicated in several diseases.[12,13]

Results from several studies indicate that angiogenesis-related miRNAs and proteins are the main components in EVs to exert their pro-angiogenic function (reviewed in Bian et al)[14] ADSC-EVs are enriched with specific protein and miRNA cargo molecules that simultaneously activate their related signal pathway to regulate the expression of angiogenic factors in endothelial cells.[13–17] EV cargo can change in response to different microenvironments, for example, EVs secreted under hypoxic conditions have been shown to contain increased expression of platelet-derived growth factor, epidermal-derived growth factor, fibroblast growth factor, and nuclear factor kappaB signaling pathway proteins and pro-angiogenic miRNAs including miR-126, miR-130a, and miR-210.[18,19]

The identity of which components of the EV proteome and miRNome responsible for the increased skin flap viability observed after H_2O_2 preconditioning of parent ADSCs has not been determined.[7] Therefore, the aims of this study were to (1) use unbiased proteomics and next-generation sequencing approaches to comprehensively characterize the protein and miRNA content of EVs released from human ADSCs under normal culture conditions (control ADSC-EVs) and from ADSCs preconditioned with H_2O_2 (H_2O_2 ADSC-EVs) and (2) determine whether H_2O_2-induced changes in EV composition can increase viability of random pattern skin flaps in an established mouse model.

MATERIALS AND METHODS

Cell Culture

Human ADSCs (ATCC PCS-500-011; American Type Culture Collection, Manassas, VA) were expanded under standard culture conditions in a complete medium [Dulbecco's Modified Eagle's Medium (DMEM) High Glucose (ThermoFisher Scientific, Waltham, MA)] containing 10% MSC-qualified fetal bovine serum (MilliporeSigma, Burlington, MA)/1×GlutaMAX/1×penicillin–streptomycin (ThermoFisher Scientific). These cells have been verified by ATCC to be multipotent, capable of differentiating into adipocytes, osteoblasts, and chondrocytes and analyzed using different cluster of differentiation (CD) markers to confirm that they meet MSC criteria as defined by the International Society for Cellular Therapy.[20] For isolation of control ADSC-EVs and H_2O_2 ADSC-EVs, culture medium was replaced with DMEM High Glucose without Phenol Red/1×GlutaMAX (ThermoFisher Scientific) containing 5% exosome-depleted fetal bovine serum (Exo-FBS; System Biosciences [SBI], Palo Alto, CA) ± 50 μM H_2O_2 when cells (at passage 5–8) reached 60%–80% confluence. Cells were cultured for an additional 65 hours, and then the medium was collected and stored at –80°C until EV isolation.

Proteomic Analysis

Proteomic analysis of control ADSC-EVs and H_2O_2 ADSC-EVs was performed by SBI utilizing SBI's ExoMS Total Exosome Protein Profiling Service. Briefly, EVs were isolated using an affinity purification strategy to remove free protein. Isolated EVs were lysed in a gel-loading buffer, and the protein concentration was determined by Qubit protein assay (ThermoFisher Scientific). EV proteins (10 μg) were processed for gel-based extraction and trypsinization to generate peptidic libraries for liquid chromatography/mass spectrometry matrix-assisted laser desorption/ionization-time-of-flight and electrospray ionization-time-of-flight mass spectrometry. Half of the gel digest was analyzed by nano-LC-MS/MS with a Waters NanoAcquity HPLC system interfaced to a ThermoFisher Q Exactive mass spectrometer. Peptides were loaded on a trapping column and eluted over a 75-μm analytical column at 350 nL/min; both columns were packed with Luna C18 resin (Phenomenex, Torrance, CA). The mass spectrometer was operated in data-dependent mode, with the Orbitrap operating at 70,000 full width at half maximum and 17,500 full width at half maximum for MS and MS/MS, respectively. The 15 most abundant ions were selected for MS/MS.

Peptide signatures were mapped to a database of known protein sequences (SwissProt Human) using Mascot (Matrix Science, Boston, MA). Mascot DAT files were parsed into Scaffold Proteome Software (Portland, OR) for validation, filtering, and to create a nonredundant list per sample. Data were filtered using 1% protein and peptide false discovery rate and requiring at least 2 unique peptides per protein. Normalized spectral abundance factor (NSAF) values were calculated based on the equation: $NSAF = (SpC/MW)/\Sigma(SpC/MW)_N$, where SpC is the spectral counts, MW is the protein molecular weight in kDa, and N is the total number of proteins. NSAF values were used to approximate the relative abundance of proteins within a given sample, and relative abundance of a given protein between samples. Functional Gene Ontology (GO) enrichment analysis of identified proteins was performed using the Functional Annotation Clustering Tool in the Database for Annotation, Visualization and Integrated Discovery (DAVID Bioinformatics Resource 6.8) using default settings.[21,22]

RNA Sequencing Analysis

Next-generation sequencing (NGS) of control ADSC-EVs and H_2O_2 ADSC-EVs was performed by SBI utilizing SBI's Exosome RNA NGS Service. Briefly, EVs were

isolated using SBI's ExoQuick precipitation method, and RNA was extracted using the SeraMir Exosome RNA Purification Column Kit (SBI). Measurement of small RNA concentration was determined using a Bioanalyzer 2100 instrument with the Agilent Small RNA Kit (Agilent Technologies, Santa Clara, CA). Small RNA libraries were constructed with the CleanTag Small RNA Library Preparation Kit (TriLink Biotechnologies, San Diego, CA). The final purified library was quantified with the High Sensitivity DNA Kit (Agilent Technologies). The libraries were pooled, and the 140–300-bp region was size selected on an 8% TBE (tris-borate-ethylenediaminetetraacetic acid) gel. The size-selected library was quantified with the High Sensitivity DNA 1000 Screen Tape Kit (Agilent Technologies) and the TailorMix HT1 qPCR Assay (SeqMatic, Fremont, CA), followed by a NextSeq High Output single-end sequencing run at SR75 using NextSeq 500/550 High Output v2 Kit (Illumina, San Diego, CA) at a depth of 5–15 million reads per sample. Data analysis was conducted using the Banana Slug Exosome RNA-seq Analysis platform using the human reference GRCh37/hg19 assembly (UCSC Genome Bioinformatics, Santa Cruz, CA). Differentially expressed miRNAs were identified using the DESeq package and reported as fold change >2 with significance considered at $P < 0.01$ (adjusted for multiple comparisons).

To determine the biological significance of differentially expressed EV miRNAs, TargetScan Release 7.2 was used to generate a list of predicted miRNA targets.[23] A cutoff of ≤ –0.3 cumulative weighted context ++ score was used to exclude weak predictions. GO enrichment analysis of predicted target genes was performed using DAVID.[21,22]

EV Isolation (Animal Experiments)

Cell debris was removed by centrifugation at 300*g* for 10 minutes and then 3,000*g* for 30 minutes. Medium was passed through a 0.22-µm filter and concentrated using a 10-kDa molecular weight Amicon Ultra-15 Centrifugal Filter (MilliporeSigma). EVs were isolated from the supernatants using ExoQuick-TC Ultra precipitation solution (SBI) according to the manufacturer's protocol and aliquots stored at –80°C before use. Aliquots of EVs were diluted in phosphate-buffered saline, and EV size and concentration were determined using nanoparticle tracking analysis by means of a NanoSight NS300 (Malvern Panalytical, Malvern, UK). Nanoparticle tracking analysis estimated the peak size of ADSC-EVs as 126 ± 8 nm and H_2O_2 ADSC-EVs as 150 ± 29 nm (n = 3 batches). Total protein concentration of EVs was determined by Qubit protein assay (ThermoFisher Scientific).

Random Pattern Skin Flap Model and In Vivo Study Design

The efficacy of control ADSC-EVs and H_2O_2 ADSC-EVs to improve viability of random pattern skin flaps was examined using an established mouse model.[2,24] The study protocol was approved by the Institutional Animal Care and Use Committee at Tripler Army Medical Center. Investigators complied with the policies as prescribed in the US Department of Agriculture Animal Welfare Act and the National Research Council's *Guide for the Care and Use of Laboratory Animals*. Facilities are fully accredited by the Association for Assessment and Accreditation of Laboratory Animal Care International.

A total of 14 male BALB/c mice (9–12 weeks old, Charles River Laboratories, Wilmington, MA) were used. Cranially based, dorsal 4 cm × 2 cm random pattern skin flaps beginning 1 cm caudal to the occipital neckline were raised in mice deeply anesthetized under isoflurane inhalation. To help create a reliable ischemic gradient from the flap base, axial vessels (if present) were crushed and a medical grade silicone sheet (approximately 0.13 mm thick) was inserted to separate the flap and avoid neovascularization from the bed. The flap was sutured in place with 4-0 nylon and left without a dressing. Animals then received intradermal injections (300 µL total volume) of control ADSC-EVs (3×10^{10} particles; n = 4 mice), H_2O_2 ADSC-EVs (3×10^{10} particles; n = 5 mice), or vehicle (n = 5 mice) at approximately 10 points throughout the proximal, middle, and distal regions of the flap. Although H_2O_2 stimulation increased the number of EVs 2.5 ± 0.4-fold (n = 3 batches), particle number was adjusted to inject equal numbers of EVs per group. Buprenorphine was administered subcutaneously (0.05 mg/kg) during surgery and orally (0.4 mg/kg mixed in 2 g/kg of hazelnut spread) every 12 hours for 2 days.

On day 7, mice were euthanized and flaps were photographed with a ruler in the field of view to enable calibration. Flap survival was determined grossly based on color, texture, and overall appearance. Sizes of viable and necrotic areas were measured using digital image analysis by 2 observers (ImageJ software, National Institutes of Health). A tissue biopsy (1 cm^2) was taken 3 mm proximal to the necrotic margin on the viable side and processed for histology.

Histologic Analysis

Tissues were fixed in formalin and embedded in paraffin, and serial sections (5 µm) were stained with hematoxylin–eosin. The number of capillaries per high-power field (400× magnification) were counted in a minimum of 10 fields per section by 2 blinded investigators and averaged.

Statistical Analysis

Data are reported as mean ± standard error of the mean. GO enrichment analysis in DAVID used a modified Fisher's exact test to determine whether genes were enriched in the annotation categories, and enrichment statistics were adjusted for multiple hypothesis testing by the Benjamini correction. All other statistical analyses were performed using SigmaPlot 11.2 software (Systat Software, San Jose, CA) with $P < 0.05$ considered significant. Comparisons among groups (viability measurements and capillary density) were made using 1-way analysis of variance (ANOVA) followed by multiple comparison testing (Holm-Sidak method) to assess differences between individual pairs of means among the groups.

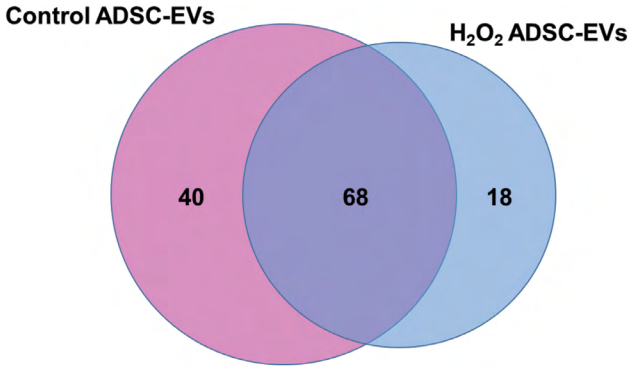

Fig. 1. Venn diagram illustrating common and unique proteins in control ADSC-EVs and H_2O_2 ADSC-EVs.

RESULTS

Protein Content of ADSC-EVs and H_2O_2 ADSC-EVs

To analyze the protein content of EVs produced by ADSCs with or without H_2O_2 stimulation, MS analysis of the proteome of control ADSC-EVs and H_2O_2 ADSC-EVs was performed. As demonstrated in the Venn diagram (Fig. 1), 68 proteins were common to both groups, 40 proteins were found only in control ADSC-EVs, and 18 proteins were found only in H_2O_2 ADSC-EVs. Functional GO enrichment analysis using DAVID software revealed that approximately 87% of identified proteins in both groups were associated with the GO term extracellular exosome (Benjamini *P* value control ADSC-EVs = 2.64×10^{-55}, H_2O_2 ADSC-EVs = 1.47×10^{-45}). Altogether, 40%–50% of identified proteins were classified as secreted proteins. The most highly enriched biological processes common to both groups were extracellular matrix organization and keratinocyte differentiation (Tables 1 and 2). Enriched GO biological processes unique to control ADSC-EVs included innate immune response and phagocytosis (Table 3). Interestingly, the major enriched GO term unique to H_2O_2 ADSC-EVs that remained significant after the adjustment for multiple hypothesis testing using the conservative Benjamini correction was constitutive photomorphogenesis 9 (COP9) signalosome, which directs the production of vascular endothelial growth factor (Table 4).[25]

Seventeen proteins identified in both groups that were altered >2-fold in H_2O_2 ADSC-EVs are listed in Table 5. Twelve (71%) of these proteins are involved in angiogenesis, and 8 (47%) have antimicrobial properties. Angiogenesis-promoting proteins enriched in H_2O_2 ADSC-EVs included transforming growth factor-beta-induced protein ig-h3, inter-alpha-trypsin inhibitor heavy chain H2, periostin, and pentraxin-related protein PTX3.[26–30]

MiRNA Content of ADSC-EVs and H_2O_2 ADSC-EVs

A total of 495 and 454 known miRNAs were identified in control ADSC-EVs and H_2O_2 ADSC-EVs, respectively.

TABLE 1. Functional Annotation Clustering Analysis of Control ADSC-EV Proteome

Term	Count	%	*P*	Benjamini *P*
Functional annotation cluster 1 enrichment score: 16.76				
GO:0005615 extracellular space	58	54.7	6.73E-37	7.14E-35
GO:0005576 extracellular region	52	49.1	2.05E-26	1.09E-24
UP_KEYWORDS secreted	53	50	8.49E-26	1.96E-23
UP_KEYWORDS signal	51	48.1	2.62E-10	2.01E-08
UP_KEYWORDS glycoprotein	50	47.2	2.14E-08	8.23E-07
Functional annotation cluster 2 enrichment score: 6.93				
GO:0018149 peptide cross-linking	10	9.4	1.91E-11	5.65E-09
GO:0030216 keratinocyte differentiation	11	10.4	3.63E-11	8.04E-09
GO:0031424 keratinization	7	6.6	4.85E-07	7.16E-05
GO:0008544 epidermis development	8	7.5	9.47E-07	1.20E-04
Functional annotation cluster 3 enrichment score: 5.55				
UP_KEYWORDS extracellular matrix	13	12.3	8.11E-09	4.68E-07
GO:0030198 extracellular matrix organization	12	11.3	3.59E-08	6.35E-06
GO:0005518 collagen binding	5	4.7	4.73E-04	0.0083
Functional annotation cluster 4 enrichment score: 5.49				
GO:0010951 negative regulation of endopeptidase activity	13	12.3	1.11E-11	4.93E-09
GO:0004867 serine-type endopeptidase inhibitor activity	9	8.5	1.25E-07	1.44E-05
UP_KEYWORDS protease inhibitor	9	8.5	2.37E-07	6.83E-06
Functional annotation cluster 5 enrichment score: 4.54				
GO:0044267 cellular protein metabolic process	8	7.5	8.56E-06	8.42E-04
Functional annotation cluster 6 enrichment score: 4.4				
GO:0002576 platelet degranulation	8	7.5	3.47E-06	3.84E-04
GO:0031093 platelet alpha granule lumen	6	5.7	1.60E-05	2.60E-04
GO:0005577 fibrinogen complex	3	2.8	0.0011	0.0128
Functional annotation cluster 7 enrichment score: 3.87				
GO:0007155 cell adhesion	12	11.3	1.28E-04	0.0075
Functional annotation cluster 8 enrichment score: 3.54				
UP_KEYWORDS antimicrobial	7	6.6	1.92E-05	2.33E-04
GO:0050832 defense response to fungus	4	3.8	6.06E-04	0.0221
GO:0042742 defense response to bacterium	6	5.7	0.0021	0.0543
Functional annotation cluster 9 enrichment score: 3.15				
GO:0016209 antioxidant activity	5	4.7	5.65E-06	2.60E-04
GO:0000302 response to reactive oxygen species	5	4.7	9.67E-05	0.0071
Functional annotation cluster 10 enrichment score: 3.04				
GO:0051092 positive regulation of NFκB transcription factor activity	7	6.6	1.77E-04	0.0092
GO:0006954 inflammatory response	10	9.4	5.76E-04	0.0219
UP_KEYWORDS innate immunity	7	6.6	0.0022	0.0150

NFκB, nuclear factor kappaB.

TABLE 2. Functional Annotation Clustering Analysis of H_2O_2 ADSC-EV Proteome

Term	Count	%	*P*	Benjamini *P*
Functional annotation cluster 1 enrichment score: 9.33				
GO:0005615 extracellular space	41	48.2	1.86E-23	1.21E-21
GO:0005576 extracellular region	37	43.5	7.46E-17	5.33E-15
UP_KEYWORDS secreted	34	40	3.20E-13	6.90E-11
UP_KEYWORDS signal	36	42.4	5.91E-06	1.42E-04
UP_KEYWORDS glycoprotein	36	42.4	4.52E-05	6.50E-04
Functional annotation cluster 2 enrichment score: 7.66				
UP_KEYWORDS heparin binding	9	10.6	2.70E-09	2.92E-07
GO:0030198 extracellular matrix organization	12	14.1	3.21E-09	7.93E-07
GO:0008201~heparin binding	9	10.6	1.18E-06	1.37E-04
Functional annotation cluster 3 enrichment score: 5.48				
UP_KEYWORDS extracellular matrix	12	14.1	8.04E-09	5.79E-07
GO:0030198 extracellular matrix organization	12	14.1	3.21E-09	7.93E-07
GO:0001501 skeletal system development	8	9.4	5.11E-06	4.73E-04
Functional annotation cluster 4 enrichment score: 4.61				
GO:0018149 peptide cross-linking	9	10.6	1.14E-10	4.24E-08
GO:0030216 keratinocyte differentiation	8	9.4	9.25E-08	1.71E-05
GO:0008544 epidermis development	7	8.2	3.89E-06	4.12E-04
Functional annotation cluster 5 enrichment score: 4.3				
GO:0010951 negative regulation of endopeptidase activity	12	14.1	1.79E-11	1.32E-08
GO:0004867 serine-type endopeptidase inhibitor activity	7	8.2	8.14E-06	3.77E-04
Functional annotation cluster 6 enrichment score: 3.55				
GO:0005178 integrin binding	6	7.1	1.67E-04	0.0035
GO:0005518 collagen binding	5	5.9	2.15E-04	0.0041
GO:0007155 cell adhesion	10	11.8	4.32E-04	0.0198
Functional annotation cluster 7 enrichment score: 3.39				
GO:0098609 cell–cell adhesion	8	9.4	3.85E-04	0.0202
Functional annotation cluster 8 enrichment score: 3.06				
GO:0004866 endopeptidase inhibitor activity	7	8.2	3.95E-08	9.16E-06
GO:0030449 regulation of complement activation	4	4.7	4.29E-04	0.0210
UP_KEYWORDS inflammatory response	5	5.9	0.0035	0.0276
Functional annotation cluster 9 enrichment score: 2.80				
GO:0042744 hydrogen peroxide catabolic process	5	5.9	2.53E-06	3.13E-04
GO:0000302 response to reactive oxygen species	4	4.7	9.36E-04	0.0400
Functional annotation cluster 10 enrichment score: 2.14				
GO:0001501 skeletal system development	8	9.4	5.11E-06	4.73E-04
GO:0030199 collagen fibril organization	4	4.7	9.36E-04	0.0400
GO:0005788 endoplasmic reticulum lumen	6	7.1	0.0019	0.0196

TABLE 3. Functional Annotation Clustering Analysis of Proteins Unique to Control ADSC-EVs

Term	Count	%	*P*	Benjamini *P*
Functional annotation cluster 1 enrichment score: 8.65				
GO:0005615 extracellular space	23	59.0	7.32E-16	4.15E-14
UP_KEYWORDS secreted	24	61.5	1.15E-14	1.60E-12
GO:0005576 extracellular region	23	59.0	3.17E-14	1.13E-12
UP_KEYWORDS signal	21	53.8	9.27E-06	4.33E-04
UP_KEYWORDS glycoprotein	21	53.8	3.75E-05	0.0011
Functional annotation cluster 2 enrichment score: 3.01				
GO:0006911 phagocytosis, engulfment	5	12.8	1.11E-06	4.53E-04
GO:0006910 phagocytosis, recognition	4	10.3	3.37E-05	0.0046
GO:0045087 innate immune response	8	20.5	4.37E-05	0.0044
UP_KEYWORDS immunoglobulin C region	3	7.7	3.43E-04	0.0080
Functional annotation cluster 3 enrichment score: 1.82				
GO:0005925 focal adhesion	6	15.4	0.0012	0.0165
GO:0005509 calcium ion binding	7	18.0	0.0038	0.1011
Functional annotation cluster 4 enrichment score: 1.56				
GO:0045087 innate immune response	8	20.5	4.37E-05	0.0044
UP_KEYWORDS innate immunity	4	10.3	0.0123	0.1341
UP_KEYWORDS inflammatory response	3	7.7	0.0320	0.2237
Functional annotation cluster 5 enrichment score: 1.28				
GO:0000502 proteasome complex	3	7.7	0.0069	0.0718
GO:0043488 regulation of mRNA stability	3	7.7	0.0227	0.5135

Using a cutoff of >2-fold change and $P < 0.01$, 2 miRNAs were increased and 12 miRNAs (including 10 anti-angiogenic miRNAs) were reduced in H_2O_2 ADSC-EVs (Table 6). Evaluation of putative target mRNAs using TargetScan Release 7.2 identified 980 predicted gene targets of these differentially expressed miRNAs. Functional GO enrichment analysis of constructed gene sets in DAVID identified the most highly enriched biological processes as transcription from RNA polymerase II promoter and embryonic skeletal system morphogenesis (Table 7).

Flap Survival and Capillary Density

On postoperative day 7, survival area was significantly larger in skin flaps of mice treated with H_2O_2 ADSC-EVs compared with vehicle ($P = 0.04$, ANOVA; Figs. 2 and 3). Increased capillary density was observed in the H_2O_2

TABLE 4. Functional Annotation Clustering Analysis of Proteins Unique to H_2O_2 ADSC-EVs

Term	Count	%	*P*	Benjamini *P*
Functional annotation cluster 1 enrichment score: 1.75				
GO:0008180 COP9 signalosome	3	16.7	4.79E-04	0.0088
UP_KEYWORDS nucleotide binding	6	33.3	0.0125	0.2309
UP_KEYWORDS ATP binding	5	27.8	0.0243	0.3474
Functional annotation cluster 2 enrichment score: 1.73				
UP_KEYWORDS Ubl conjugation	6	33.3	0.0103	0.3019
UP_KEYWORDS isopeptide bond	5	27.8	0.01218	0.2729
Functional annotation cluster 3 enrichment score: 1.59				
UP_KEYWORDS acetylation	10	55.6	6.51E-04	0.0654
UP_KEYWORDS methylation	5	27.8	0.0080	0.3401
UP_KEYWORDS Ubl conjugation	6	33.3	0.0103	0.3019
GO:0098609 cell–cell adhesion	3	16.7	0.0301	0.8627
GO:0098641 cadherin binding involved in cell–cell adhesion	3	16.7	0.0338	0.8172
Functional annotation cluster 4 enrichment score: 1.28				
GO:0006413 translational initiation	3	16.7	0.0083	0.5560
GO:0044822 poly(A) RNA binding	5	27.8	0.0235	0.9050
Functional annotation cluster 5 enrichment score: 1.26				
GO:0005576 extracellular region	8	44.4	3.64E-04	0.0089
GO:0005615 extracellular space	6	33.3	0.0064	0.0905
GO:0010951 negative regulation of endopeptidase activity	3	16.7	0.0065	0.7210

TABLE 5. Proteins Identified in Both Control ADSC-EVs and H_2O_2 ADSC-EVs that Were Altered (>2-Fold Change) in H_2O_2 ADSC-EVs

Proteins Upregulated in H_2O_2-ADSC-EVs	Abbreviation	MW (kDa)	UniProtKB Acc. #*	Fold Change	Function	Reference
Histone H4	H4_HUMAN	11	P62805	4.35	Major antimicrobial peptide on skin released from sebaceous glands	31
Transforming growth factor-beta-induced protein ig-h3	BGH3_HUMAN	75	Q15582	3.59	Collagen-binding extracellular matrix protein; involved in vascular remodeling; pro-angiogenic	26
Inter-alpha-trypsin inhibitor heavy chain H2	ITIH2_HUMAN	106	P19823	2.63	Serum protein that promotes hyaluronan-mediated angiogenesis in tissue injury	27
Filaggrin-2	FILA2_HUMAN	248	Q5D862	2.39	Essential for normal keratinocyte differentiation; C-terminal fragments are antimicrobial peptides	32, 33
Periostin	POSTN_HUMAN	93	Q15063	2.39	Extracellular matrix protein that promotes angiogenesis and tissue repair	28
Thrombospondin-1	TSP1_HUMAN	129	P07996	2.32	Potent endogenous inhibitor of angiogenesis	34
Pentraxin-related protein PTX3	PTX3_HUMAN	42	P26022	2.22	Pattern recognition molecule of innate immune system; promotes angiogenesis after stroke	29, 30
Annexin A5	ANXA5_HUMAN	36	P08758	2.09	Inhibits tumor angiogenesis; probe for apoptosis	35
Proteins Downregulated in H_2O_2-ADSC-EVs	**Abbreviation**	**MW (kDa)**	**UniProtKB Acc. #**	**Fold Change**	**Function**	**Reference**
Plakophilin-1	PKP1_HUMAN	83	Q13835	–5.56	Structural component of desmosomes important for cell–cell adhesion	36
Vitamin D-binding protein	VTDB_HUMAN	53	P02774	–2.65	Inhibits angiogenesis; antiendothelial activity	37
Apolipoprotein B-100	APOB_HUMAN	516	P04114	–2.65	Contains cryptic host defense peptides	38
Lactotransferrin	TRFL_HUMAN	78	P02788	–2.51	Inhibits angiogenesis in colon tumor model; iron-binding antimicrobial protein	39, 40
Serotransferrin	TRFE_HUMAN	77	P02787	–2.51	Inhibits angiogenesis in pancreatic tumor model; iron-binding antimicrobial protein	41, 42
Alpha-fetoprotein	FETA_HUMAN	69	P02771	–2.51	Modulates expression of VEGF; pro-angiogenic	43
Fatty acid-binding protein 5	FABP5_HUMAN	15	Q01469	–2.09	Promotes angiogenesis and activates IL6/STAT3/VEGFA pathway	44
Dermcidin	DCD_HUMAN	11	P81605	–2.09	Antimicrobial peptide	45
Hornerin	HORN_HUMAN	282	Q86YZ3	–2.08	Protein in skin that contains cationic antimicrobial peptides; pro-angiogenic	46, 47

*UniProtKB Acc. #, UniProt Knowledgebase Accession Number.

ADSC-EV group compared to that in the other groups ($P < 0.001$, ANOVA; Figs. 4 and 5). Increased vessel diameter was also apparent in tissues treated with H_2O_2 ADSC-EVs (Fig. 5).

DISCUSSION

The use of stem cell-derived EVs has gained much attention as an emerging approach for therapeutic angiogenesis in ischemic diseases.[14] In fact, EVs are currently being tested in clinical trials in patients with acute ischemic stroke, type 1 diabetes mellitus, and macular holes.[8] Recently, Bai et al determined that preconditioning ADSCs with a low concentration of H_2O_2 improved the pro-angiogenic properties of secreted EVs in vitro and in vivo in a model of skin flap transplantation, suggesting that H_2O_2 may induce EVs to exhibit an enhanced pro-angiogenic capacity for cell-free therapeutic applications.[7] In this study, comprehensive proteomic and miRNA

TABLE 6. Differentially Expressed miRNAs (>2-Fold Change, $P < 0.01$) in H_2O_2 ADSC-EVs Compared to Control ADSC-EVs

miRNA	Fold Change	Normalized Abundance Control ADSC-EVs	Normalized Abundance H_2O_2 ADSC-EVs	*P*	Role in Angiogenesis	Reference
hsa-miR-10395-5p	13.76	2.17	29.86	0.0007	Unknown	
hsa-miR-10395-3p	13.56	2.17	29.42	0.0008	Unknown	
hsa-miR-24-3p	–3.42	397.69	116.12	<0.0001	Antiangiogenic	13
hsa-miR-16-5p	–3.08	75.23	24.44	0.0025	Antiangiogenic	13
hsa-miR-93-5p	–2.64	88.65	33.53	0.0044	Pro-angiogenic	48
hsa-miR-31-5p	–2.56	509.43	199.31	<0.0001	Pro-angiogenic, antiangiogenic	49, 50
hsa-miR-23a-3p	–2.46	441.80	179.85	<0.0001	Pro-angiogenic	13
hsa-miR-152-3p	–2.27	156.95	69.07	0.0011	Antiangiogenic	51
hsa-miR-122-5p	–2.23	894.20	401.27	<0.0001	Antiangiogenic	52
hsa-miR-134-5p	–2.19	223.78	102.32	0.0064	Antiangiogenic	53
hsa-miR-221-3p	–2.19	12206.98	5582.17	<0.0001	Antiangiogenic	13
hsa-miR-196a-5p	–2.17	173.55	79.87	0.0063	Antiangiogenic	54
hsa-miR-23b-3p	–2.11	255.23	120.97	0.0005	Antiangiogenic	55
hsa-miR-222-3p	–2.11	871.46	413.91	<0.0001	Antiangiogenic	13

TABLE 7. Biological Processes Enriched among the Genes Predicted to Be Targeted by miRNAs that Were Downregulated (>2-Fold Change, $P < 0.01$) in H_2O_2 ADSC-EVs Compared to Control ADSC-EVs

GO Term	Count	%	*P*	Benjamini *P*
GO:0006366 transcription from RNA polymerase II promoter	53	5.4	2.75E-06	0.0092
GO:0048704 embryonic skeletal system morphogenesis	12	1.2	2.95E-06	0.0050
GO:0045893 positive regulation of transcription, DNA templated	52	5.3	6.66E-06	0.0075
GO:0009952 anterior/posterior pattern specification	16	1.6	1.28E-05	0.0108
GO:1900740 positive regulation of protein insertion into Mitochondrial membrane involved in apoptotic signaling pathway	10	1.0	1.36E-05	0.0092
GO:0014911 positive regulation of smooth muscle cell migration	8	0.8	4.15E-05	0.0232
GO:0008284 positive regulation of cell proliferation	46	4.7	4.27E-05	0.0205
GO:0048863 stem cell differentiation	9	0.9	4.58E-05	0.0192
GO:0045944 positive regulation of transcription from RNA Polymerase II promoter	80	8.2	5.72E-05	0.0213
GO:0030335 positive regulation of cell migration	24	2.4	8.03E-05	0.0269
GO:0000122 negative regulation of transcription from RNA Polymerase II promoter	62	6.3	1.01E-04	0.0307
GO:0006468 protein phosphorylation	44	4.5	1.08E-04	0.0300

analyses revealed that exposure to an H_2O_2-induced oxidative stress microenvironment altered the expression of several angiogenic and antimicrobial proteins and miRNAs in ADSC-EVs. We also verified that H_2O_2 ADSC-EVs increased microvascular density and viability of random pattern skin flaps in vivo.

Functional enrichment analysis of proteins found only in H_2O_2 ADSC-EVs identified COP9 signalosome as the primary enriched GO term unique to H_2O_2 ADSC-EVs. The COP9 signalosome is a highly conserved multimeric protein complex with kinase activity that cooperates with the ubiquitin/26S proteasome system in the regulation of stability of important cellular proteins.[25] The COP9 signalosome has been shown to direct the production of vascular endothelial growth factor, a major mediator of angiogenesis, through c-Jun signaling in tumor cells, thereby promoting angiogenesis.[25] Upregulation of proteins involved in this complex therefore may be 1 mechanism by which H_2O_2 ADSC-EVs enhance angiogenesis.

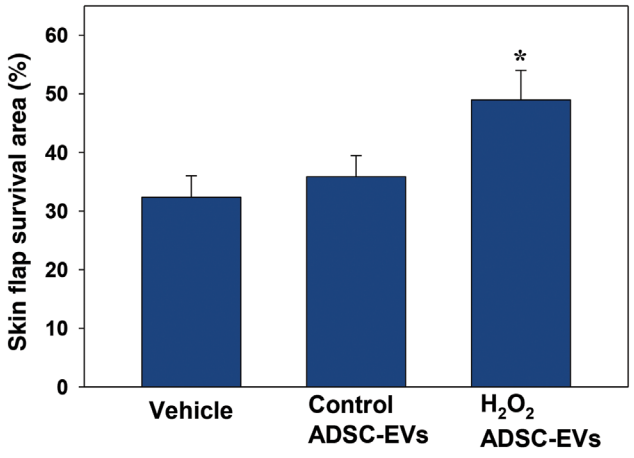

Fig. 2. Quantitative analysis of skin flap survival area. *$P < 0.05$ vs vehicle.

Angiogenesis is well known to be a complex process that is regulated by a variety of angiogenic stimulators and inhibitors.[13] H_2O_2 pretreatment resulted in the upregulation and downregulation of several pro-angiogenic and antiangiogenic proteins and miRNAs (listed in Tables 5 and 6), thereby influencing this intricate balance. Angiogenesis-promoting proteins enriched in ADSC-EVs after H_2O_2 stimulation included the extracellular matrix proteins periostin and transforming growth factor-beta-induced protein ig-h3, and pentraxin-related protein PTX3 and inter-alpha-trypsin inhibitor heavy chain H2, previously shown to promote wound healing and vascular remodeling.[26–30] Of the 14 differentially expressed miRNAs, 10 are considered to be antiangiogenic and all were downregulated in H_2O_2 ADSC-EVs, consequently increasing angiogenesis via release

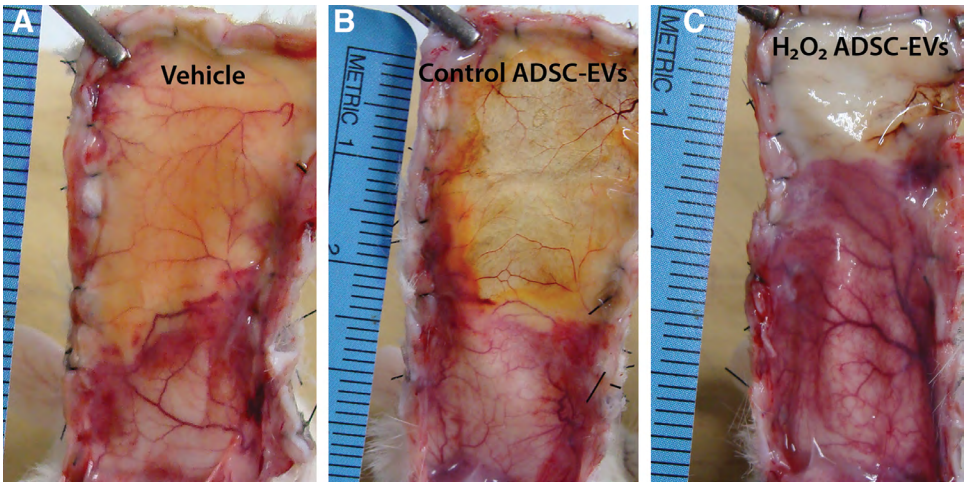

Fig. 3. Representative images of skin flaps injected with vehicle (A), control ADSC-EVs (B), and H2O2 ADSC-EVs (C) (elevated to display the underside) on postoperative day 7. Note the increased area of viable tissue within the flap treated with H_2O_2 ADSC-EVs (C).

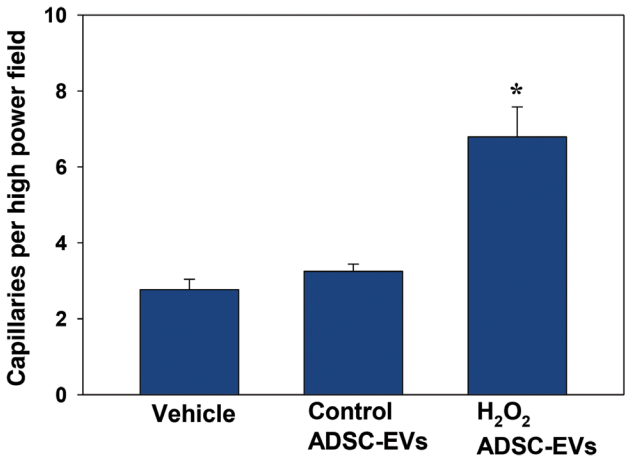

Fig. 4. Quantitative analysis of capillary density. *$P < 0.05$ vs vehicle and control ADSC-EVs.

of inhibition.[13,50–55] Both groups contained known pro-angiogenic miRNAs that were not differentially expressed such as abundant levels of miR-21. MiR-21 has been shown to have antibacterial, antiinflammatory, and proliferative roles in a diabetic infected wound model and has been proposed as a promising intervention target for the treatment of refractory wounds such as diabetic foot ulcers.[56]

Results from this study also suggest that ADSC-EVs may benefit wound healing and infection prevention of skin flaps through their antimicrobial peptide content. Twenty-four antimicrobial peptides and proteins important in innate immunity were identified in ADSC-EVs, including dermcidin, lipocalin-1, lysozyme C, neutrophil defensin 1, prolactin-inducible protein, psoriasin (S100A7), calprotectin (S100A8/A9), histone H4, lactotransferrin, and hornerin, to name a few. These peptides are known to have activities against various Gram-positive

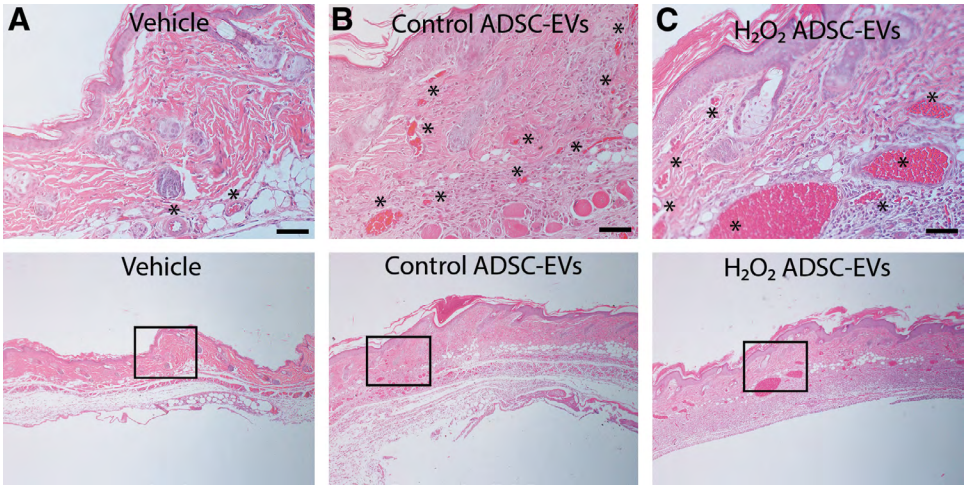

Fig. 5. Representative hematoxylin–eosin-stained sections of skin flaps injected with vehicle (A), control ADSC-EVs (B), and H_2O_2 ADSC-EVs (C). Top panels are magnified views of corresponding boxes in bottom panels. Scale bar = 50 μm. Blood vessels are denoted by *.

and Gram-negative bacteria, viruses, and fungi, and likely are responsible for the antimicrobial properties of MSCs observed by us and others.[57,58] Some of these peptides have been identified in sweat EVs, suggesting a role in skin immunity.[59] Although it has been postulated that MSC-EVs contain active agents with potential antimicrobial effects, a paucity of data exists regarding the antimicrobial peptide cargo of ADSC-EVs and how it may be affected by different microenvironments.[60] In general, antimicrobial peptides and proteins were reduced in H_2O_2 ADSC-EVs. However, histone H4 and filaggrin-2, whose peptides are important in antimicrobial defense of the skin, were upregulated in H_2O_2 ADSC-EVs.[31–33] Interestingly, pentraxin-related protein PTX3, which was also upregulated in H_2O_2 ADSC-EVs, is an essential soluble pattern recognition molecule of the innate immune system and a key regulator of angiogenesis that exerts dual functions involving both antimicrobial resistance and tissue repair.[29,30]

Although the therapeutic benefits of EVs seem highly encouraging in preclinical models, technical challenges currently exist in this exciting new field that must be resolved before EV-based therapeutics may be incorporated into clinical practice. One of the major challenges is the efficient production of EVs in a clinically applicable scale. Other obstacles include a lack of consensus (1) on the best method to isolate and purify EVs, (2) on the compositions of EVs from different sources or different culture conditions, and (3) as to how to quantitate the EVs.[61] Nevertheless, Mendt et al in conjunction with Codiak Biosciences have recently developed a process for the production of Good Manufacturing Practice-grade EVs derived from MSCs.[62] Using a Quantum bioreactor culture system, they demonstrated successful Good Manufacturing Practice-grade production, scalability, EV stability, and consistent in vitro and in vivo efficacy in preclinical models of pancreatic cancer.[62] In addition, EVs can be lyophilized and stored at 4°C without compromising stability for 36 months and are easily reconstituted, thereby demonstrating great promise as an "off-the-shelf" therapeutic.

CONCLUSIONS

ADSC-EVs hold immense potential as an allogeneic, "off-the-shelf" cell-free therapeutic for skin flap transplantation offering the benefits of stem cell therapy while representing a theoretically safer alternative. The broad repertoire of angiogenic and antimicrobial proteins and miRNAs in ADSC-EVs, which are altered after H_2O_2 preconditioning, likely contributes to their favorable therapeutic effects observed on skin flap survival. Further investigation is needed to determine the relative importance of particular miRNAs and proteins and their affected signaling pathways in flap recovery.

Lisa M. Pierce, DSc
Department of Clinical Investigation
Tripler Army Medical Center1 Jarrett White Road
Honolulu, HI 96859-5000
E-mail: lisa.m.pierce.civ@mail.mil

REFERENCES

1. Matsen CB, Mehrara B, Eaton A, et al. Skin flap necrosis after mastectomy with reconstruction: a prospective study. *Ann Surg Oncol.* 2016;23:257–264.
2. Lu F, Mizuno H, Uysal CA, et al. Improved viability of random pattern skin flaps through the use of adipose-derived stem cells. *Plast Reconstr Surg.* 2008;121:50–58.
3. Atef A, Shaker A, Sadek EY, et al. The optimal timing of adipose derived stem cells injection to improve skin flap survival in a rat model. *Eur J Plast Surg.* 2018;41:387–394.
4. Reichenberger MA, Heimer S, Schaefer A, et al. Adipose derived stem cells protect skin flaps against ischemia-reperfusion injury. *Stem Cell Rev Rep.* 2012;8:854–862.
5. Uysal AC, Mizuno H, Tobita M, et al. The effect of adipose-derived stem cells on ischemia-reperfusion injury: immunohistochemical and ultrastructural evaluation. *Plast Reconstr Surg.* 2009;124:804–815.
6. Pu CM, Liu CW, Liang CJ, et al. Adipose-derived stem cells protect skin flaps against ischemia/reperfusion injury via IL-6 expression. *J Invest Dermatol.* 2017;137:1353–1362.
7. Bai Y, Han YD, Yan XL, et al. Adipose mesenchymal stem cell-derived exosomes stimulated by hydrogen peroxide enhanced skin flap recovery in ischemia-reperfusion injury. *Biochem Biophys Res Commun.* 2018;500:310–317.
8. Phinney DG, Pittenger MF. Concise review: MSC-derived exosomes for cell-free therapy. *Stem Cells.* 2017;35:851–858.
9. Yin K, Wang S, Zhao RC. Exosomes from mesenchymal stem/stromal cells: a new therapeutic paradigm. *Biomark Res.* 2019;7:8.
10. Zheng G, Huang R, Qiu G, et al. Mesenchymal stromal cell-derived extracellular vesicles: regenerative and immunomodulatory effects and potential applications in sepsis. *Cell Tissue Res.* 2018;374:1–15.
11. Seo Y, Kim HS, Hong IS. Stem cell-derived extracellular vesicles as immunomodulatory therapeutics. *Stem Cells Int.* 2019;2019:5126156.
12. Ha TY. MicroRNAs in human diseases: from autoimmune diseases to skin, psychiatric and neurodegenerative diseases. *Immune Netw.* 2011;11:227–244.
13. Tiwari A, Mukherjee B, Dixit M. MicroRNA key to angiogenesis regulation: miRNA biology and therapy. *Curr Cancer Drug Targets.* 2018;18:266–277.
14. Bian X, Ma K, Zhang C, et al. Therapeutic angiogenesis using stem cell-derived extracellular vesicles: an emerging approach for treatment of ischemic diseases. *Stem Cell Res Ther.* 2019;10:158.
15. Gai C, Carpanetto A, Deregibus MC, et al. Extracellular vesicle-mediated modulation of angiogenesis. *Histol Histopathol.* 2016;31:379–391.
16. Chen J, Liu Z, Hong MM, et al. Proangiogenic compositions of microvesicles derived from human umbilical cord mesenchymal stem cells. *Plos One.* 2014;9:e115316.
17. Gong M, Yu B, Wang J, et al. Mesenchymal stem cells release exosomes that transfer miRNAs to endothelial cells and promote angiogenesis. *Oncotarget.* 2017;8:45200–45212.
18. Anderson JD, Johansson HJ, Graham CS, et al. Comprehensive proteomic analysis of mesenchymal stem cell exosomes reveals modulation of angiogenesis via nuclear factor-kappab signaling. *Stem Cells.* 2016;34:601–613.
19. Namazi H, Mohit E, Namazi I, et al. Exosomes secreted by hypoxic cardiosphere-derived cells enhance tube formation and increase pro-angiogenic miRNA. *J Cell Biochem.* 2018;119:4150–4160.
20. Dominici M, Le Blanc K, Mueller I, et al. Minimal criteria for defining multipotent mesenchymal stromal cells. The international society for cellular therapy position statement. *Cytotherapy.* 2006;8:315–317.

21. Huang da W, Sherman BT, Lempicki RA. Systematic and integrative analysis of large gene lists using DAVID bioinformatics resources. *Nat Protoc.* 2009;4:44–57.
22. Huang da W, Sherman BT, Lempicki RA. Bioinformatics enrichment tools: paths toward the comprehensive functional analysis of large gene lists. *Nucleic Acids Res.* 2009;37:1–13.
23. Agarwal V, Bell GW, Nam JW, et al. Predicting effective miRNA target sites in mammalian mRNAs. *eLife.* 2015;4:e05005.
24. Park IS, Mondal A, Chung PS, et al. Prevention of skin flap necrosis by use of adipose-derived stromal cells with light-emitting diode phototherapy. *Cytotherapy.* 2015;17:283–292.
25. Pollmann C, Huang X, Mall J, et al. The constitutive photomorphogenesis 9 signalosome directs vascular endothelial growth factor production in tumor cells. *Cancer Res.* 2001;61:8416–8421.
26. Newman AC, Nakatsu MN, Chou W, et al. The requirement for fibroblasts in angiogenesis: fibroblast-derived matrix proteins are essential for endothelial cell lumen formation. *Mol Biol Cell.* 2011;22:3791–3800.
27. Garantziotis S, Zudaire E, Trempus CS, et al. Serum inter-alpha-trypsin inhibitor and matrix hyaluronan promote angiogenesis in fibrotic lung injury. *Am J Respir Crit Care Med.* 2008;178:939–947.
28. Kim BR, Kwon YW, Park GT, et al. Identification of a novel angiogenic peptide from periostin. *Plos One.* 2017;12:e0187464.
29. Doni A, Garlanda C, Mantovani A. Innate immunity, hemostasis and matrix remodeling: PTX3 as a link. *Semin Immunol.* 2016;28:570–577.
30. Rajkovic I, Wong R, Lemarchand E, et al. Pentraxin 3 promotes long-term cerebral blood flow recovery, angiogenesis, and neuronal survival after stroke. *J Mol Med (Berl).* 2018;96:1319–1332.
31. Lee DY, Huang CM, Nakatsuji T, et al. Histone H4 is a major component of the antimicrobial action of human sebocytes. *J Invest Dermatol.* 2009;129:2489–2496.
32. Pendaries V, Le Lamer M, Cau L, et al. In a three-dimensional reconstructed human epidermis filaggrin-2 is essential for proper cornification. *Cell Death Dis.* 2015;6:e1656.
33. Hansmann B, Schröder JM, Gerstel U. Skin-derived C-terminal filaggrin-2 fragments are pseudomonas aeruginosa-directed antimicrobials targeting bacterial replication. *Plos Pathog.* 2015;11:e1005159.
34. Lawler PR, Lawler J. Molecular basis for the regulation of angiogenesis by thrombospondin-1 and -2. *Cold Spring Harb Perspect Med.* 2012;2:a006627.
35. Zhang X, Huo L, Jin H, et al. Anti-cancer activity of annexin V in murine melanoma model by suppressing tumor angiogenesis. *Oncotarget.* 2017;8:42602–42612.
36. Fischer-Kešo R, Breuninger S, Hofmann S, et al. Plakophilins 1 and 3 bind to FXR1 and thereby influence the mRNA stability of desmosomal proteins. *Mol Cell Biol.* 2014;34:4244–4256.
37. Kalkunte S, Brard L, Granai CO, et al. Inhibition of angiogenesis by vitamin D-binding protein: characterization of anti-endothelial activity of DBP-maf. *Angiogenesis.* 2005;8:349–360.
38. Gaglione R, Cesaro A, Dell'Olmo E, et al. Effects of human antimicrobial cryptides identified in apolipoprotein B depend on specific features of bacterial strains. *Sci Rep.* 2019;9:6728.
39. Li HY, Li M, Luo CC, et al. Lactoferrin exerts antitumor effects by inhibiting angiogenesis in a HT29 human colon tumor model. *J Agric Food Chem.* 2017;65:10464–10472.
40. Yen CC, Shen CJ, Hsu WH, et al. Lactoferrin: an iron-binding antimicrobial protein against Escherichia coli infection. *Biometals.* 2011;24:585–594.
41. Liang G, Butterfield C, Liang J, et al. Beta-35 is a transferrin-derived inhibitor of angiogenesis and tumor growth. *Biochem Biophys Res Commun.* 2011;409:562–566.
42. Bruhn KW, Spellberg B. Transferrin-mediated iron sequestration as a novel therapy for bacterial and fungal infections. *Curr Opin Microbiol.* 2015;27:57–61.
43. Meng W, Li X, Bai Z, et al. Silencing alpha-fetoprotein inhibits VEGF and MMP-2/9 production in human hepatocellular carcinoma cell. *Plos One.* 2014;9:e90660.
44. Pan L, Xiao H, Liao R, et al. Fatty acid binding protein 5 promotes tumor angiogenesis and activates the IL6/STAT3/VEGFA pathway in hepatocellular carcinoma. *Biomed Pharmacother.* 2018;106:68–76.
45. Senyürek I, Paulmann M, Sinnberg T, et al. Dermcidin-derived peptides show a different mode of action than the cathelicidin LL-37 against staphylococcus aureus. *Antimicrob Agents Chemother.* 2009;53:2499–2509.
46. Gerstel U, Latendorf T, Bartels J, et al. Hornerin contains a linked series of ribosome-targeting peptide antibiotics. *Sci Rep.* 2018;8:16158.
47. Gutknecht MF, Seaman ME, Ning B, et al. Identification of the S100 fused-type protein hornerin as a regulator of tumor vascularity. *Nat Commun.* 2017;8:552.
48. Liang L, Zhao L, Zan Y, et al. Mir-93-5p enhances growth and angiogenesis capacity of HUVECs by down-regulating EPLIN. *Oncotarget.* 2017;8:107033–107043.
49. Kang T, Jones TM, Naddell C, et al. Adipose-derived stem cells induce angiogenesis via microvesicle transport of miRNA-31. *Stem Cells Transl Med.* 2016;5:440–450.
50. Ye J, Zhu J, Chen H, et al. A novel lncRNA-LINC01116 regulates tumorigenesis of glioma by targeting VEGFA. *Int J Cancer.* 2019.
51. Marques JHM, Mota AL, Oliveira JG, et al. Melatonin restrains angiogenic factors in triple-negative breast cancer by targeting miR-152-3p: *in vivo* and *in vitro* studies. *Life Sci.* 2018;208:131–138.
52. Wang Y, Xing QF, Liu XQ, et al. Mir-122 targets VEGFC in bladder cancer to inhibit tumor growth and angiogenesis. *Am J Transl Res.* 2016;8:3056–3066.
53. Zhang L, Lv Z, Xu J, et al. MicroRNA-134 inhibits osteosarcoma angiogenesis and proliferation by targeting the VEGFA/VEGFR1 pathway. *Febs J.* 2018;285:1359–1371.
54. Pin AL, Houle F, Fournier P, et al. Annexin-1-mediated endothelial cell migration and angiogenesis are regulated by vascular endothelial growth factor (VEGF)-induced inhibition of miR-196a expression. *J Biol Chem.* 2012;287:30541–30551.
55. Hannafon BN, Carpenter KJ, Berry WL, et al. Exosome-mediated microRNA signaling from breast cancer cells is altered by the anti-angiogenesis agent docosahexaenoic acid (DHA). *Mol Cancer.* 2015;14:133.
56. Li T, Ma Y, Wang M, et al. Platelet-rich plasma plays an antibacterial, anti-inflammatory and cell proliferation-promoting role in an *in vitro* model for diabetic infected wounds. *Infect Drug Resist.* 2019;12:297–309.
57. Patel S, Akhtar N. Antimicrobial peptides (amps): the quintessential 'offense and defense' molecules are more than antimicrobials. *Biomed Pharmacother.* 2017;95:1276–1283.
58. Criman ET, Kurata WE, Matsumoto KW, et al. Bone marrow-derived mesenchymal stem cells enhance bacterial clearance and preserve bioprosthetic integrity in a model of mesh infection. *Plast Reconstr Surg Glob Open.* 2016;4:e751.
59. Wu CX, Liu ZF. Proteomic profiling of sweat exosome suggests its involvement in skin immunity. *J Invest Dermatol.* 2018;138:89–97.
60. Alcayaga-Miranda F, Cuenca J, Khoury M. Antimicrobial activity of mesenchymal stem cells: current status and new perspectives of antimicrobial peptide-based therapies. *Front Immunol.* 2017;8:339.
61. Pacienza N, Lee RH, Bae EH, et al. *In vitro* macrophage assay predicts the *in vivo* anti-inflammatory potential of exosomes from human mesenchymal stromal cells. *Mol Ther Methods Clin Dev.* 2019;13:67–76.
62. Mendt M, Kamerkar S, Sugimoto H, et al. Generation and testing of clinical-grade exosomes for pancreatic cancer. *JCI Insight.* 2018;3:e99263.